PERGAMON

International Journal of Heat and Mass Transfer 42 (1999) 3983–4003

International Journal of HEAT and MASS TRANSFER

www.elsevier.com/locate/ijhmt

Turbulent Rayleigh–Bénard convection in low Prandtl-number fluids[1]

S. Horanyi[a], L. Krebs[b], U. Müller[b,*]

[a]*Atomic Energy Research Institute, Budapest, Hungary*

[b]*Forschungszentrum Karlsruhe GmbH, Institut für Angewandte Thermo- und Fluiddynamik, P.O. Box 3640, 76021 Karlsruhe, Germany*

Received 8 June 1998; received in revised form 5 February 1999

Abstract

An experimental investigation of Rayleigh–Bénard convection in liquid sodium has been performed in cylindrical test cells with aspect ratios between 20 and 4.5 for a range of Rayleigh numbers $10^4 < Ra < 5 \times 10^6$. The Prandtl number is between $6.0 \times 10^{-3} \pm 0.1 \times 10^{-3}$. For low Rayleigh number $Ra < 10^4$ the dimensionless heat flux, Nu is mainly conduction controlled and close to 1; a correlation $Nu = 0.115 \times Ra^{0.25}$ describes the observations adequately for $2 \times 10^4 < Ra < 5 \times 10^6$. It is shown that the Nusselt numbers are smaller for sodium than for other fluids with larger Prandtl numbers such as mercury and helium. This contrasts with the relation $Nu \sim Ra^{2/7} Pr^{1/7}$ recently proposed by Siggia [High Rayleigh number convection. Ann. Rev. Fluid Mech. (1994)] but conforms with a relation $Nu \sim (Ra\ Pr)^{1/4}$ for low Prandtl number fluids derived by Jones et al. [Axisymmetric convection in a cylinder. J. Fluid Mech. 73 (1976) 353–358] and with recent numerical simulations of low Prandtl number convection by Vercicco and Camussi [Transitional regimes of low-Prandtl thermal convection in a cylindrical cell. Phys. Fluids 9 (5) (1997) 1287–1295]. The heat transfer as well as the statistical properties of the turbulent convection are significantly influenced by mode transitions in the test cell of small aspect ratio. The formation of thermal boundary layers occurs only at high Rayleigh numbers of the order $Ra \gtrsim 10^6$. An instability in these thermal boundary layers triggers a new mode of large scale fluctuating motion. The analysis of the temperature time signals shows that the temperature field behaves essentially dissipative up to Rayleigh numbers $Ra \sim 5 \times 10^6$.

1. Introduction

An improved understanding of turbulent-free convection in liquids of very low Prandtl number (i.e. high thermal conductivity) such as liquid metals and other high temperature molten materials is highly desirable for several applications in nuclear power engineering and more recently in materials processing industries. It is equally important for explaining and modeling certain geo-planetary or astrophysical observations for instance the granular structure of the solar surface or planetary and stellar magnetic fields. A well-defined and experimentally accessible free convection system is the Rayleigh–Bénard convection in plane horizontal liquid layers with large temperature differences between top and bottom. In recent years several novel experiments have been conducted in high Rayleigh–Bénard

* Corresponding author. Tel.: +49 (7247) 82 3450; fax: +49 (7247) 82 4837.

E-mail address: ulrich.mueller@iatf.fzk.de (U. Müller)

[1] This paper is dedicated to Prof. Dr.-Ing. Jürgen Zierep on the occasion of his 70th birthday.

0017-9310/99/$ - see front matter
PII: S0017-9310(99)00059-9

Nomenclature

A	area of heat transfer
d	diameter of test cell
E	power density spectrum
F	flatness
h	height of test cell
Nu	Nusselt number
Pr	Prandtl number
PDF	probability density function
PSD	power spectrum density
Ptn	resistance thermometer n
Q	electrical power
R	radius of test cell
Ra	Rayleigh number
RMS	root mean square of temperature
S	skewness
T	mean temperature
TCn	thermocouple n
v	velocity

Greek symbols

β	coefficient of thermal expansion
Δ	difference
ϵ	dissipation
κ	thermal diffusivity
λ	thermal conductivity
ν	kinematic viscosity
τ_K	Kolmogoroff time scale
τ_θ	Batchelor time scale
Φ	correlation function

Subscripts

b	buoyancy
n	normalized
s	signal
sod	sodium
T	temperature

convection by different research groups [4–10]. Most of these experiments were performed in containers with an aspect ratio one and with either water or helium as test fluids whose Prandtl numbers are $Pr \simeq 7$ and 0.7, respectively. Only Cioni et al. [11,12] and Takeshita et al. [13] report experiments in mercury with $Pr \simeq 0.025$. The new experiments have, on the one hand, advanced the available heat transfer data base into the very high Rayleigh number regime $Ra \lesssim 10^{15}$ and, moreover, provided new local mean and statistical data of the temperature and velocity field of buoyant turbulent flows. On the other hand, they have initiated modeling efforts for turbulent flow which center around modifications of scaling laws for heat transfer and spectral dynamics of the temperature due to the interaction of large scale 'cellular' motion and small scale turbulence in sheared thermal boundary layers [4,14–17]. New concepts such as 'soft' and 'hard' turbulence have been introduced based on the structure of the probability density function measured in test containers of small height to diameter ratio and at high Rayleigh numbers [4]. New 'structure' functions were proposed to characterize the intermittent behaviour of turbulent flows. We believe that the new experimental and theoretical approach to thermal turbulence needs completion if not correction with regard to the influence of low Prandtl number and aspect ratio. We therefore resumed the former experimental work of Kek [18] on heat transfer through liquid sodium layers and have extended the previous investigations to a Rayleigh number range $2.5 \times 10^5 < Ra < 4.5 \times 10^6$. New experiments were performed in cylindrical containers of

Table 1
Heat transfer correlations and range of validity

$Nu = 0.069 Ra^{0.33} Pr^{0.074}$	$1.5 \times 10^5 < Ra < 4 \times 10^7$ (for any fluid)	Globe and Dropkin [20]
$Nu = 0.147 Ra^{0.257}$	$10^3 < Ra < 5 \times 10^5$ (mercury)	Rossby [21]
$Nu = 0.078 Ra^{0.32}$	$4.8 \times 10^6 < Ra < 4 \times 10^7$ (sodium)	McDonald and Connoly [22]
$Nu = 0.140 Ra^{0.26}$	$7 \times 10^6 < Ra < 4.5 \times 10^8$ (mercury)	Cioni et al. [12]
$Nu = 0.44 Ra^{0.20}$	$4.5 \times 10^8 < Ra < 2.1 \times 10^9$ (mercury)	Cioni et al. [12]
$Nu = 0.155 Ra^{0.27}$	$2 \times 10^6 < Ra < 8 \times 10^7$ (mercury)	Takeshita et al. [13]
Model correlations:		
$Nu = 0.17 (Ra\ Pr)^{1/3}$	$Ra \gg 1700$, $Pr < 1$	Kraichnan [23]
$Nu = 0.175 Ra^{1/4}$	$[Ra\ Pr]^{1/2} \gg 1$	Busse and Clever [24]
$Nu = 0.27 Ra^{2/7} Pr^{-1/7}$	$(10^7$–$10^8) Pr^{3/5} < Ra < (10^{13}$–$10^{15}) Pr^4$	Shraiman and Siggia [15]
$Nu = 0.25 (Ra\ Pr)^{2/7}$	$10^6 < Ra < 10^9$, $Pr \ll 1$	Cioni et al. [8]

aspect ratio, diameter to height, of 20 and 4.5. In this article mainly the results of the experiment in the larger test cell with $d/h = 4.5$ are presented, because the instrumentation within the sodium layer was more complete. However, some results obtained for the test cell with $d/h = 20$ are included in the graphs for the Nusselt numbers and RMS-values for the temperature fluctuations.

This paper presents new data for the heat transfer through sodium layers and for the time averaged temperature distribution across the layer. Furthermore, statistical data of temperature signals are presented and discussed such as root mean square values (RMS), probability density functions (PDF) and power spectrum density functions (PSD) for different heating powers. Data from cross-correlation measurements between temperature probes provide a clue about the buoyant velocity in the layer.

2. Brief survey of the literature

An extensive survey of the current state of knowledge on turbulent Bénard convection has been compiled by Siggia [1]. A summary of the empirical and theoretical heat transfer correlations applicable for low Prandtl number convection has been given by Kek and Müller [19]. Here we list in Table 1 some frequently used heat transfer correlations applicable to low Prandtl number flow.

It has been debated by several research groups, whether the heat transfer correlation in form of the 1/3 power law describes the experimental observations properly within the experimental error bounds or whether a power of $2/7 \approx 0.286$ applies as derived by Castaing et al. [4]. It is not obvious a priori why careful measurements in water conducted by Krishnamurti [9] and by Goldstein et al. [10] do not confirm strictly to the $Nu \sim Ra^{2/7}$ power law observed in experiments by Heslot et al. [5] and in those by Threllfall [25], Chavanne et al. [26] in helium and by Cioni et al. [12] in water and mercury. But there is significant evidence from the experimental findings of Krishnamurti, that the realized different large scale convection patterns in the different test cells of different experimenters give rise to the discrepancies in the heat transfer correlations.

Moreover, it is evident that the correlation of Shraiman and Siggia [15] in Table 1 fails to predict properly the heat transfer for very low values of the Prandtl number because of its singular behavior for $Pr \to 0$. Cioni et al. [8] have modified the Shraiman and Siggia model to account for the low Prandtl number case. They find $Nu = 0.25\ (Ra \times Pr)^{2/7}$ for $Pr < 0.3$. However, their argument that thermal plumes released from the thermal boundary layers are accelerated in the mixing layer is not obvious.

Temperature distributions across the layer height in turbulent convection have been measured repeatedly in the past in air, water and silicon oil by Deardorf and Willis [27], Goldstein and Chu [28,29], Somerscales and Gazda [30]. Velocity measurements for very high Rayleigh number flow are scarce. To our knowledge only mean velocity profiles have been measured by Garon and Goldstein [31], Kikuchi et al. [32] and Tilgner et al. [6]. In a few cases local mean velocities at the layer mid-height have been obtained by temperature correlation measurements or particle image velocimetry in helium and water, see for example Tanaka and Miyata [33], Sano et al. [34]. Statistical properties of turbulent convection are available from several research groups for air, helium and water. Generally, the data for the temperature field are far more complete than those for the velocity field. RMS-values and power density spectra for the temperature and velocity field have been given for air as a test fluid by Deardorf and Willis [35] in an intermediate range of Rayleigh numbers $6.3 \times 10^5 < Ra < 1.0 \times 10^7$. For water and for one particular value $Ra = 1.1 \times 10^9$ Tilgner et al. [6] have obtained RMS-values for the temperature and velocity field in the vicinity of the cooled upper boundary. Power density spectra (PDS) and probability density functions (PDF) of the temperature time signals have been provided for the test fluid helium and a wide range of Rayleigh numbers by Libchaber and his group [5,34]. Their measurements have initiated a sequel of theoretical research activities in the field of highly turbulent convection. A particular new phenomenon is the observed transition of the probability density functions for temperature from a Guassian distribution to an exponential one in convection experiments at very high Rayleigh numbers. After Castaing et al. [4] the related turbulent flow field is termed either 'soft' or 'hard', respectively, depending on a Gaussian or exponential shape of the probability density function of the temperature fluctuations. The universality of this criterion has been criticized by other experimentalists, e.g. by Salomon and Gollub [7].

Compared with the available experimental investigations in fluids of moderate Prandtl number the data base for statistical evaluations of turbulent flow from experiments in liquid metals is very limited. A first attempt to evaluate temperature time signals from mercury experiments in terms of power density spectra was undertaken by Rossby [21]. Recently some more investigations were performed by Kek [18], Cioni et al. [11,8] and Takeshita et al. [13] who provide data such as the temperature variance, the skewness and flatness, the probability density function and power density spectra employing time signal recordings from thermocouples inside the layer. Kek performed his measure-

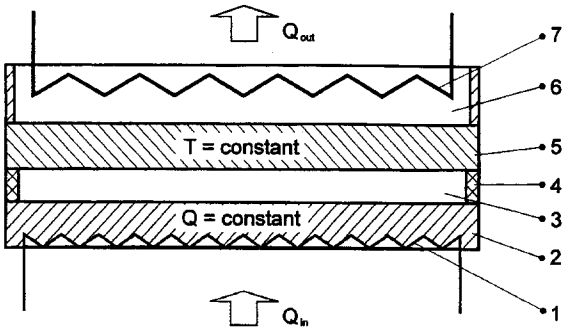

Fig. 1. Schematic sketch of the test apparatus: electrical power supply (1); heating plate, copper (2); sodium layer (3); side wall, nickel (4); cooling plate, copper (5); boiling cooler, oil (6); heat exchanger, water/oil (7).

ments in liquid sodium in a relatively low Rayleigh number range $Re < 2.4 \times 10^5$ while Cioni's mercury data apply for $7 \times 10^6 < Ra < 2.1 \times 10^9$ and Takeshita's for $10^6 < Ra < 10^8$. There are in general only very few measurements available for free convection in low Prandtl number fluids. These facts encouraged us to continue the sodium experiments first started by Kek [18].

3. The experimental set up, measuring technique and data evaluation

The convection apparatus, the measuring technique and an error analysis of the control instrumentation including a discussion of possible heat losses have been described elsewhere in detail, see Kek [18] and Kek and Müller [19]. We therefore limit ourselves to outline the essential features only. The test apparatus is depicted schematically in Fig. 1. The dimensions of the circular test chamber are 500 mm in diameter and 15.5, 25, 46.5 and 110 mm in height. Most of the new experiments are conducted with a layer height of 110 mm. The experiments are carried out at a mean temperature level between 550–570 K in the sodium and for heating powers of 1–17 kW at the bottom plate. The temperature of the cooling plate is kept constant using a boiling cooler and oil as a coolant. The temperature difference is measured across the sodium layer by six pairs of Pt-100 resistance thermometers placed in bore holes which are radially drilled into the top and bottom copper plates of the test apparatus at different depths. Two rakes equipped with nine thermocouples each at different vertical elevations are placed near the center of the test cell to measure the vertical temperature profile in the layer. A sketch of the resistance thermometers, the thermocouple rake and their locations is shown in Figs. 2(a) and (b). In order to control the uniformity of the test section temperature, nine more thermocouples are located at the perimeter of the test section in three sets, each consisting of three thermocouples, fixed in a 120° subdivision on the side wall of the container. The thermocouples in each set are arranged in a vertical line at intervals of 3 cm. In addition, a prong fitted with eight thermocouples at particular positions and at equal distances from each other was moved repeatedly during the test runs into the center bore hole of the cooling plate to measure the local temperature distribution of the upper boundary along radius. Also, during special tests all the Pt-100 resistance thermometers were moved radially in their particular bore holes to the same radial position to check the temperature uniformity of the upper and lower boundaries in the azimuthal direction, see Fig. 2(a). The integral properties of the test, the Rayleigh number Ra, the mean heat transfer coefficient $\bar{\alpha}$ and the mean Nusselt number $\overline{Nu}$ are evaluated in the same manner as in the paper by Kek and Müller [19]. The following definitions are used:

$$Ra = \frac{\beta g h^3}{\kappa \nu} \Delta T_{\mathrm{sod}},$$

$$\bar{a} = \frac{Q}{A} \frac{1}{6} \sum_{j=1}^{6} \frac{1}{\Delta T_{\mathrm{sod}}^{(j)}},$$

$$\overline{Nu} = \frac{\bar{a} h}{\lambda_{\mathrm{sod}}}. \tag{1}$$

Here β is the coefficient of thermal expansion, g the acceleration of gravity, h the layer height, κ the thermal diffusivity, ν the kinematic viscosity, Q the total heating power, A the total heated sodium surface, ΔT_{sod} the arithmetic mean temperature difference across the sodium layer and λ_{sod} the thermal conductivity of sodium. ΔT_{sod} is evaluated from the difference between opposite pairs of resistance thermometers, allowing for the temperature differences inside the copper plates between the thermometers and the surface in contact with the sodium. The individual temperature differences $\Delta T_{\mathrm{sod}}(j)$ are calculated assuming a constant mean heat flux at the heating plate. The mean heat transfer coefficient $\bar{\alpha}$ is determined as the arithmetic mean of the local heat transfer coefficients

$$a_j = \frac{Q}{A} \frac{1}{\Delta T_{\mathrm{sod}}^{(j)}}.$$

Temperature time signals are recorded from the Pt-100 resistance thermometers and the thermocouples inside the copper plates and the thermocouples protruding into the sodium layer from the two rakes. Steel sheathed Ni–Cr–Ni thermocouples of tip diameter 0.25 mm were used. Their undamped frequency re-

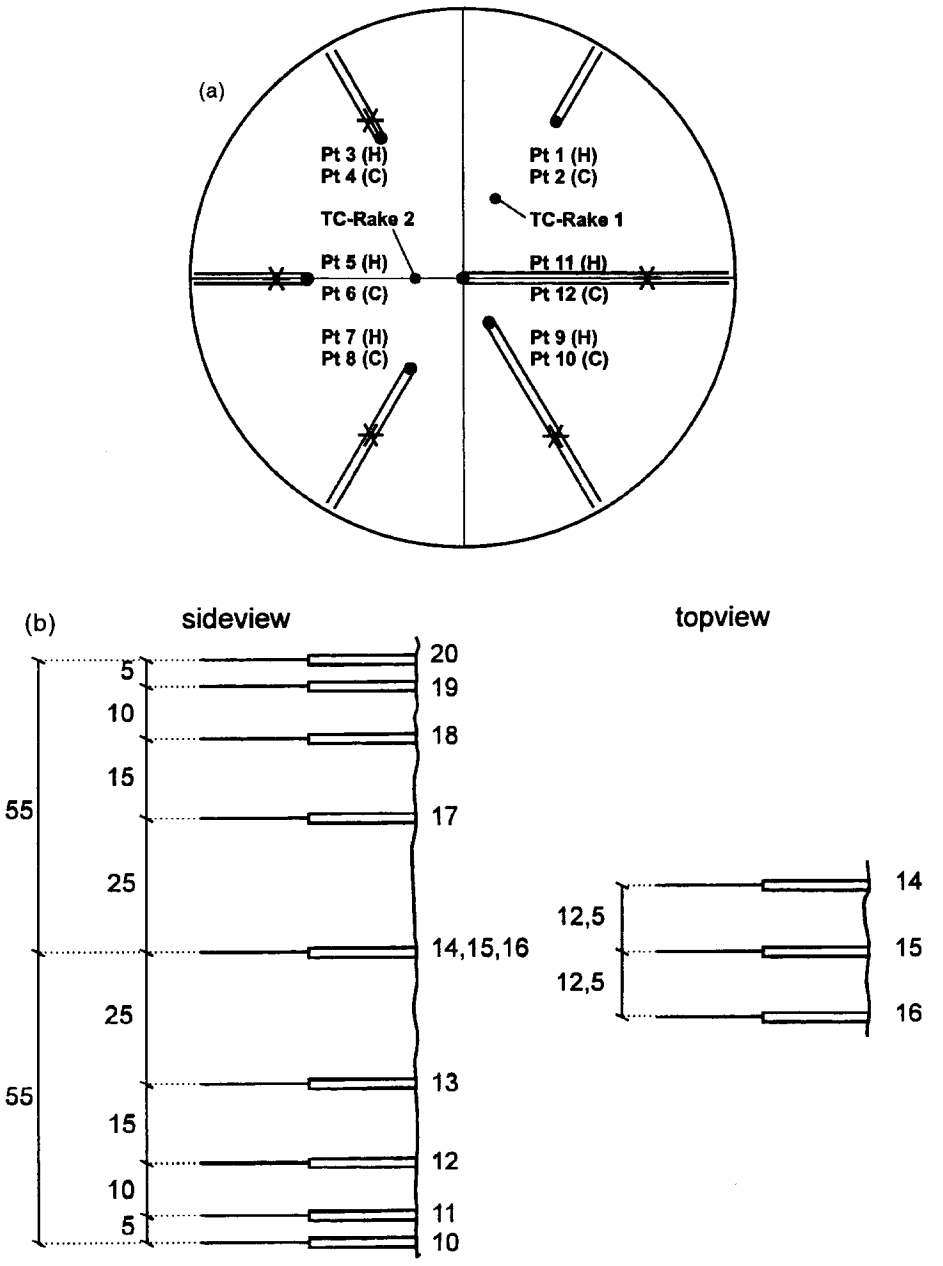

Fig. 2. (a) Radial positions of Pt-100 resistance thermometers in the heating (H) and cooling (C) plates and of thermocouple rakes TC-rake 1 and TC-rake 2 in the sodium layer, respectively. Symbol (●) denotes end position of the Pt-100 within each bore hole, symbol (×) position at equal distance from the rim. (b) Axial positions of thermocouples on the TC-rake 2.

sponse is about 40 Hz [36]. The signals are then evaluated for the RMS-value, the skewness S and flatness F. Additionally, auto- and cross-correlations Φ and power density spectra (PSD) are calculated. The definition and evaluation procedure for these functions can be found in any textbook on turbulence statistics, e.g. Lumley [37]. The sampling frequency is varied from 1–10 Hz depending on the heating power and, hence, the observed time scale in the temperature signal, in order to resolve signal properties up to 5 Hz. The evaluation is performed with the aid of a commercial software package PlotIT [38]. Up to 10,000 points are generally taken for evaluating the statistical properties and then processed for the plots. For mean

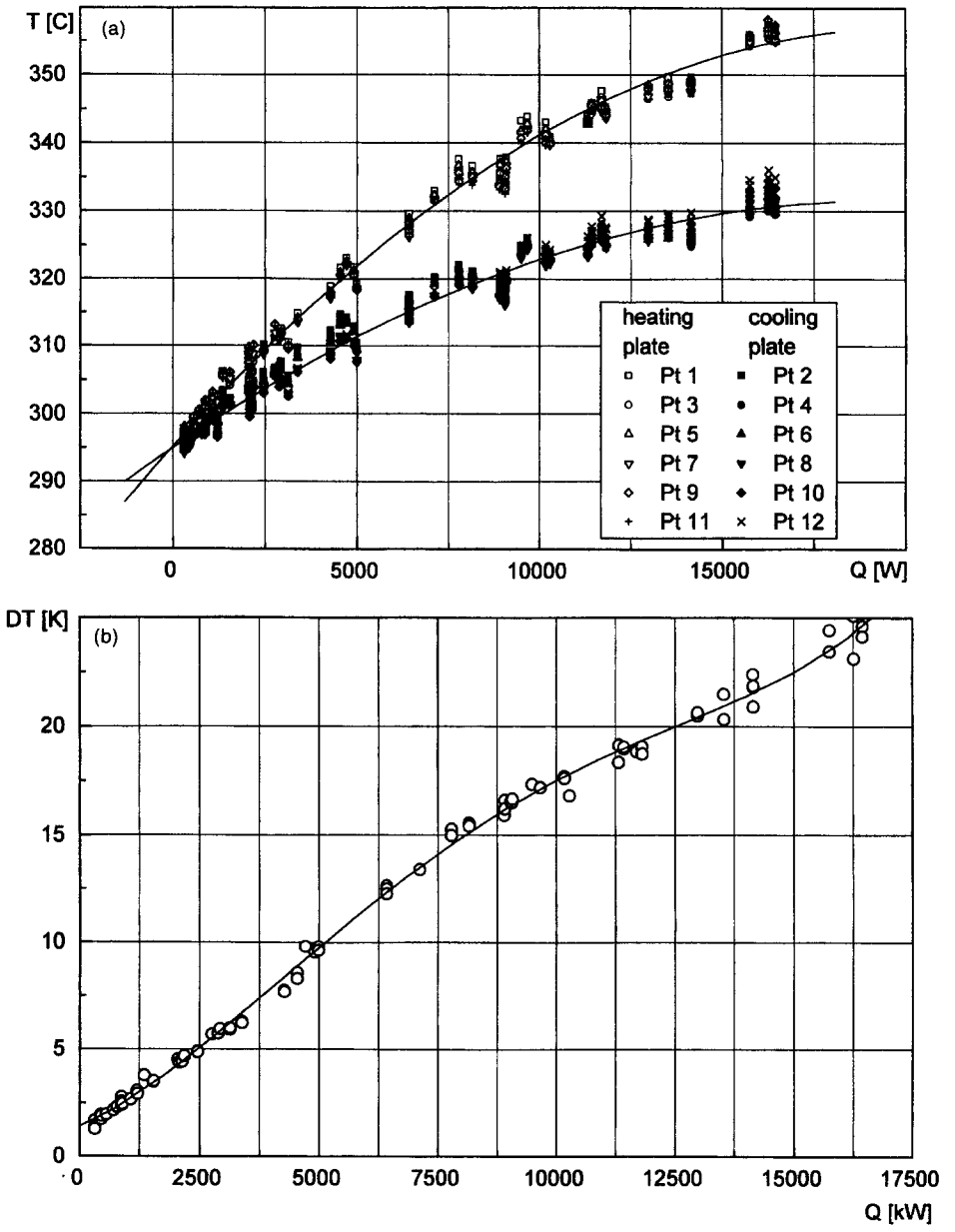

Fig. 3. (a) Local surface temperatures of heating and cooling plate. (b) Mean temperature differences between the surfaces of heating and cooling plate versus heating power.

values 150 points are usually taken with a sampling rate of 0.2 Hz which means an averaging time of 750 s.

4. Results

4.1. Heat transfer

The local mean surface temperatures (averaging time 750 s) can be seen in Fig. 3(a). They are evaluated from the measurements by the six pairs of opposite Pt-100 thermometers in the cooling and heating plates at the tip of the bore holes (see Fig. 2(a)) for increasing heating powers. Moreover, this graph shows the temperature variation at the copper plates in the radial direction. A closer look to the data points shows that the temperature variations are generally larger for a given heating power at the cooling plate. The mean

temperature difference across the layer is given in Fig. 3(b) as a function of the heating power. It is determined by averaging the temperature differences from all six pairs of resistance thermometers at an actual heating power. The graph shows that the heat transfer mode is subject to significant changes in the range between $10 < \Delta T\,[\mathrm{K}] < 15$. This has an impact on the Nusselt–Rayleigh number relation. The radial variation (compare Fig. 2(a)) of the time averaged local temperature difference across the sodium layer and the associated Ra number can also be recognized in Fig. 4 for different power levels. The functional dependence of the fitting curves changes in the range $7 \times 10^5 < Ra < 2 \times 10^6$ from a curve of mostly negative curvature to one with an inflection point and at $Ra \approx 2.4 \times 10^6$ to a persistent positive slope. We suggest that this feature is associated with a transition between two different flow modes in the sodium layer. This will be discussed in more detail in Section 4.2. The non-uniformity of the temperature distribution, measured in the heating and cooling copper plates, indicates an intrinsic difficulty of heat transfer investigations in sodium layers. Since the heat conductivities of sodium and copper are of similar size (see below Section 4.2), ideal thermal boundary conditions such as constant temperature or constant heat flux conditions cannot be achieved. In particular, because of the convection flow pattern the temperature field in the sodium layer will have a feed back on the temperature distribution in the confining horizontal copper boundaries.

The dimensionless heat transfer graph $Nu(Ra)$ can be evaluated using the data base of Figs. 3(a) and (b) and Eq. (1). The results are presented in Figs. 5(a) and (b). The data plot in Fig. 5(a) indicates clearly two different heat transfer modes, one in a range $Ra \leq 1 \times 10^6$, the other for $Ra \geq 1.5 \times 10^6$ with a sudden decrease of the convective heat transfer in between. This drastic change in the $Nu(Ra)$ graph is reflected in the slope changes of the heat transfer graph in Fig. 3(b). The transition occurs at heating powers between 5 and 6 kW which correspond to Rayleigh numbers of 1.2×10^6 and 1.9×10^6. We consider this 'jump' in the Nusselt–Rayleigh number relation another characteristic feature for a mode transition of the convection pattern which proceeds in a spatially and temporally fluctuating manner in this weakly turbulent flow regime. The transition zone corresponds to the change of shape in the radial temperature distribution of Fig. 4. In Fig. 5(b) the new data are plotted together with heat transfer data for sodium obtained by Kek [18] and Horanyi [39] in containers of large aspect ratio $d/h = 33$ and 11, respectively. In the range $2 \times 10^4 < Ra < 10^6$ the data are well represented by the correlation

$$Nu = 0.115 Ra^{0.25}. \tag{2}$$

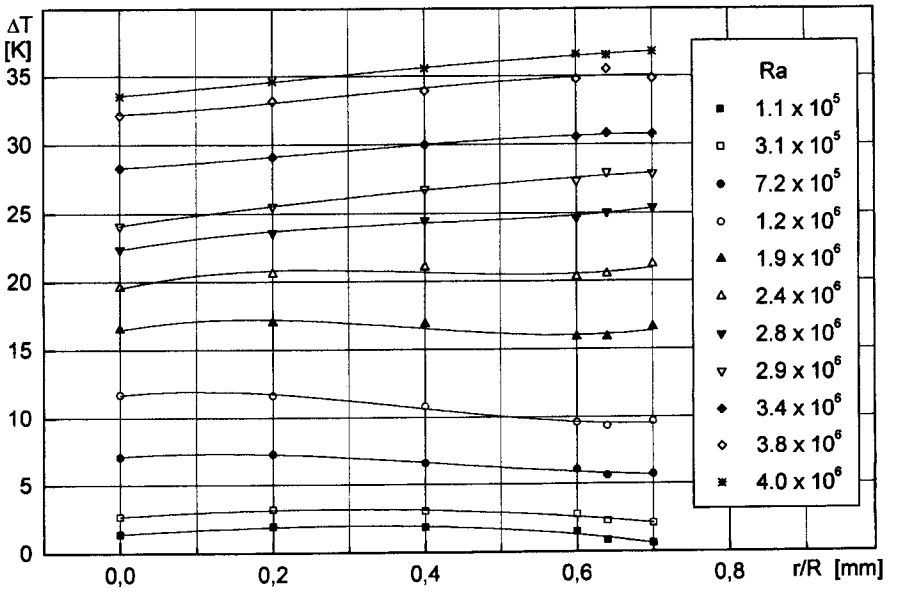

Fig. 4. Radial profiles of the mean temperature differences measured by the six pairs of opposite Pt-100 thermometers between the surfaces of the heating and cooling plates.

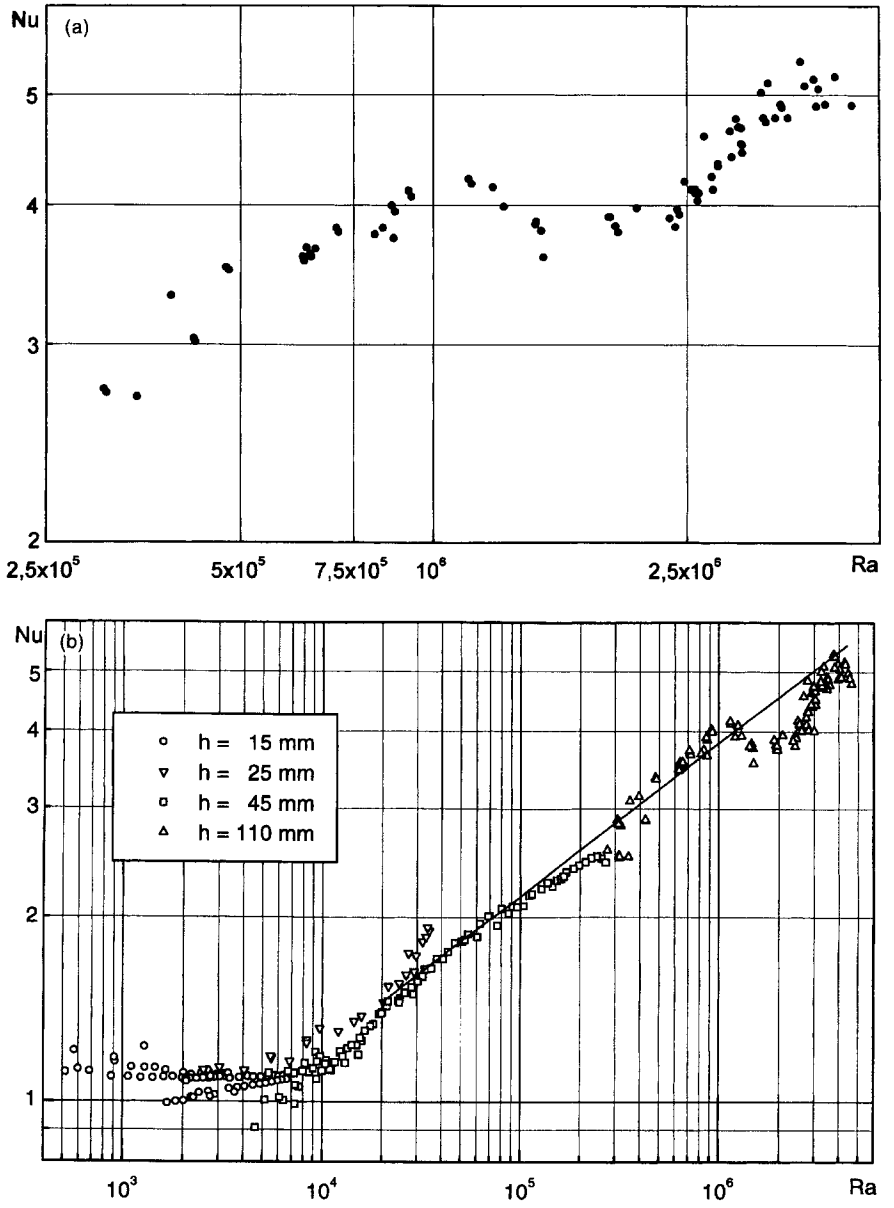

Fig. 5. (a) Dimensionless heat transfer correlation $Nu(Ra)$ evaluated for the aspect ratio $d/h = 4.5$. (b) Dimensionless heat transfer correlation $Nu(Ra)$ evaluated for the aspect ratios 33 (○), 20 (▽), 11 (□) and 4.5 (△).

One may consider the Rayleigh numbers $10^6 < Ra < 3 \times 10^6$ as a range in which the heat flux is first perturbed by a change of the convection mode in a test chamber of rather small aspect ratio $d/h = 4.5$ but finally recovers and extrapolate the above correlation also to the extended range $Ra \leq 4.5 \times 10^6$. Further experiments for even higher Rayleigh numbers are required to corroborate this conjecture.

4.2. Large scale flow structures

A striking observation of the experiments is the fact that the temperature fluctuations from the turbulent sodium flow are well sensed by the Pt-100 resistance thermometers located in the copper plates at a distance of 25 mm from the wetted surface. This is not surprising as the thermal conductivity of copper ($\lambda_{cu} \approx 380$ W/mK) is only about five times larger than that of

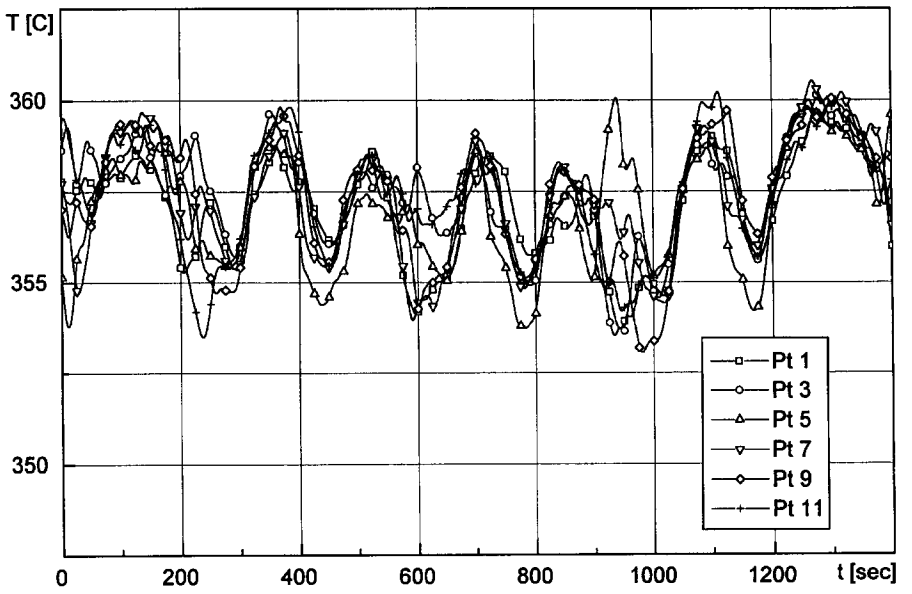

Fig. 6. Temperature histories of the six Pt-100 thermometers each separated by 60° on a radial position $r/R = 0.7$. The signals are recorded at a Rayleigh number $Ra = 3.5 \times 10^6$ corresponding to a heating power of 14 kW.

sodium ($\lambda_{Na} \approx 75$ W/mK). Moreover, the thermal diffusivities of copper and sodium are nearly equal. Thus, the experimental situation is far from the usual isothermal boundary condition.[2] Fig. 6 shows a typical temperature history recorded by six Pt-100 thermometers in the heating plate at a Rayleigh number $Ra = 3.5 \times 10^6$ or equivalently for a heating power of 14 kW in a time interval of 1400 s. During this particular experiment all the sensors are placed in the bore holes at the same radial distance of 80 mm from the rim of the test section but separated azimuthally by a 60° subdivision (see Fig. 2(a)). Clearly, the copper has a damping effect on the high frequency content of the original temperature fluctuations, but the low frequency structure of all six temperature traces show a high coherency. Cross-correlations of the signals recorded by the different resistance thermometers result in correlation coefficients ranging between 0.69 and 0.86. The same observations have been made for other heating powers. The very low frequencies in fluctuating Bénard convection can be associated with a slow motion of cellular patterns. We infer from the coherency of the signals that the flow pattern in the sodium layer maintains a high degree of axisymmetry. This axisymmetric coherency and the relatively small aspect ratio of the test chamber suggest that the convection pattern consists of two fluctuating concentric ring rolls. This type of flow pattern has been observed in the past in cylindrical containers heated from below, if for example the convection is simultaneously forced by small radial temperature gradients in the top or bottom plates in the vicinity of the vertical side wall [40–43]. A sketch of the conjectured pattern is given in Fig. 7. This conjecture of a double roll structure gets some support from an analysis of the measured temperature distribution in the bounding heated copper plates. This temperature distribution can be seen in Fig. 3(a) for different heating powers. In particular for $Q > 10^4$ W an obvious depression in the temperature distribution is visible in a radius range $r/R \sim 0.5$ and higher temperatures are observed in the center and the rim area indicating an up-, down- and up-flow distribution along the radius. For small heating powers a similar observation is less obvious and—as one reviewer rightly commented—a direct three-dimensional numerical analysis of this heat transfer problem could possibly resolve the remaining uncertainties concerning the actual flow structures.

In order to assess the magnitude of the vertical velocity in the sodium layer, cross-correlations were performed between the signals of thermocouples TC13 and TC17 of rake 2 (see Fig. 2(b)). The signal velocity is shown as a function of the heating power in Fig. 8. For Rayleigh numbers $Ra < 1 \times 10^6$ we find a velocity in downward direction in the center of the test chamber; for $Ra \geq 2 \times 10^6$ the flow direction is upward. This finding corroborates our previous conjecture obtained from discussions of Figs. 3 and 4,

[2] The relevant Biot number $Bi = \lambda_{cu}/\lambda_{Na} \times h/d$ has a value of about 10.

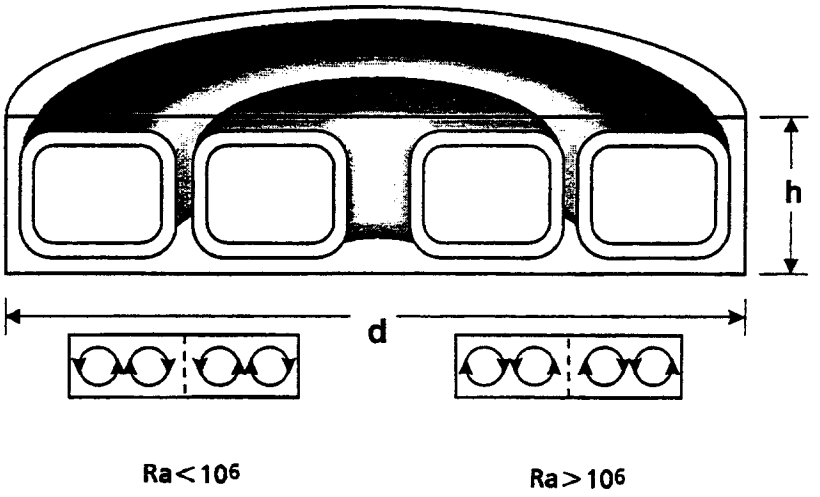

Fig. 7. Schematic sketch of the flow pattern for an aspect ratio d/h = 4.5 of the sodium layer. After Fig. 8 there is a flow reversal at $Ra \approx 10^6$ ($Q \sim 4000$ W).

namely that a change of the flow pattern occurs in the power range $4000 < Q < 6000$ W, i.e. $1.2 \times 10^6 < Ra < 2 \times 10^6$. The measured velocities vary between a few and 100 mm/s. This is consistent with an evaluation of the buoyant velocity v_b obtained from the measured Rayleigh number at corresponding heating powers and the given Prandtl number by $v_b = \nu/h \times (Ra/Pr)^{1/2}$. We obtain, for instance, a velocity of $v_b = 11.3$ cms^{-1} for $Ra = 4 \times 10^6$ (compare Section 4.3). This corresponds to the measured signal velocity of $v_s \simeq 13$ cms^{-1}. There is a reasonable agreement in the order of magnitude, if one takes into account the uncertainties which exist for the temperature correlation measurements in sodium with its large thermal diffusivity [44,45]. In spite of the quantitative uncertainties in cross-correlation measurements the change from negative to positive velocities is obvious.

Temperature distributions across the sodium layer, time averaged for 5000 s, are presented in Fig. 9. The profiles are obtained from the nine thermocouples of rake probe 2 near the cell center. The most obvious feature in this graph is the formation of pronounced

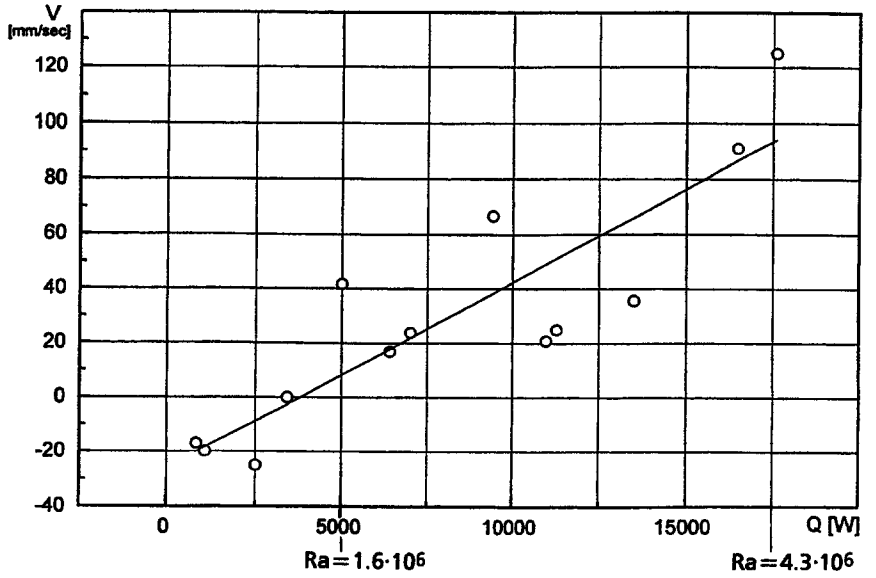

Fig. 8. Signal velocity of temperature fluctuations obtained from cross-correlation of temperature signals of TC13 and TC17.

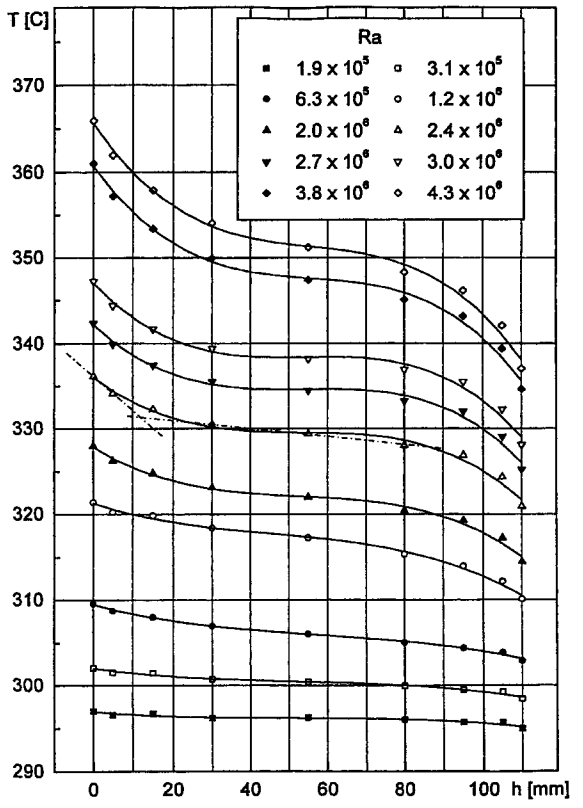

Fig. 9. Mean temperature profiles for different Ra across the sodium layer at the position of TC-rake 2.

thermal boundary layers at the heating and cooling plates and a weakly decreasing temperature in the middle region of the layer for heating rates beyond 4 kW corresponding to $Ra > 1.1 \times 10^6$. There is no temperature gradient reversal in the core of the layer as observed by Chu and Goldstein [29] in experiments with water. The formation of the thermal boundary layers seems to correlate with the rapid change in the Nusselt–Rayleigh number correlation of Fig. 5. The thickness of the boundary layer varies roughly between 10 and 20 mm. A crude evaluation of the boundary layer thickness by linear extrapolation of the temperature gradients at the wall and the center of the layer (see Fig. 9) indicates that the thermal boundary layer becomes unstable first at the heated bottom for $Ra \approx 2.4 \times 10^6$. Indeed, a rough estimate of a Rayleigh number, based on the evaluated thermal boundary layer thickness and the temperature drop across it at the bottom plate, suggests that its value is significantly above $Ra_\delta \simeq 1100$ which is the critical value for a heated horizontal layer with 'free' upper surface. The onset of the boundary layer instability conforms with the drastic variation of the Nusselt number in Fig. 5. We conjecture that the instability of the thermal boundary layer triggers a change in the mode of convection. It is well-known from convection experiments in containers with small aspect ratio [46] that small perturbations such as instabilities of thermal boundary layers can trigger transitions between neighboring convection modes of similar energy levels.

4.3. Local turbulence properties

Temperature signals recorded by three thermocouples of the TC rake probe 2 (see Fig. 2(b)) are presented in Figs. 10(a)–(c). The thermocouples are located at mid-height of the layer (T_{15}), in direct contact with the heated copper plate (T_{10}) and in contact with the cooled copper plate (T_{20}). The small scale, short term fluctuations with periods lower than 10 s exhibit the highest intensity at the layer mid height (see Fig. 10(a)). This is consistent with the idea, that the short term fluctuations are damped near the upper and lower boundaries. Otherwise Fig. 10(a) shows a long term uniform temporal behavior. This long term character of the temperature signals changes drastically for the Rayleigh numbers $Ra = 2.9 \times 10^6$ and $Ra = 4.3 \times 10^6$ displayed in Figs. 10(b) and (c). A new long period fluctuations of 300–400 s occurs which modulates the high frequency temperature fluctuations. Moreover, the intensities of the low frequency mode recorded by the three different thermocouples are nearly equal. This observation suggests that the two different time scales of the temperature history may be associated with two relevant length scales of the experiment in this range of Rayleigh numbers, namely the thickness of the thermal boundary layer and the container dimensions related to the large scale wavelength of the roll pattern. The small scale fluctuations in the order of a few seconds are consistent with the time for thermal diffusion across a thermal boundary layer of about 10–20 mm and a thermal diffusivity for sodium of 7×10^{-5} m^2 s^{-1} (see Figs. 9 and 12 for an assessment of the boundary layer thickness). The large scale fluctuation of the ring roll pattern may be imagined as a quasi periodic fluctuation of the free cell boundary located in a range near $r/R \approx 0.5$ which is generally associated with a fluctuation of the intensity of the large scale convection velocity and thus generally correlates to the turn over time of an individual convection cell. But we shall see below that in our case the turn over time of a few seconds is not compatible with the observed long period fluctuations.

The large scale temperature fluctuations are also sensed by the resistance thermometers in the copper plates. For the highest Rayleigh number $Ra = 4.3 \times 10^6$ temperature signals are recorded by

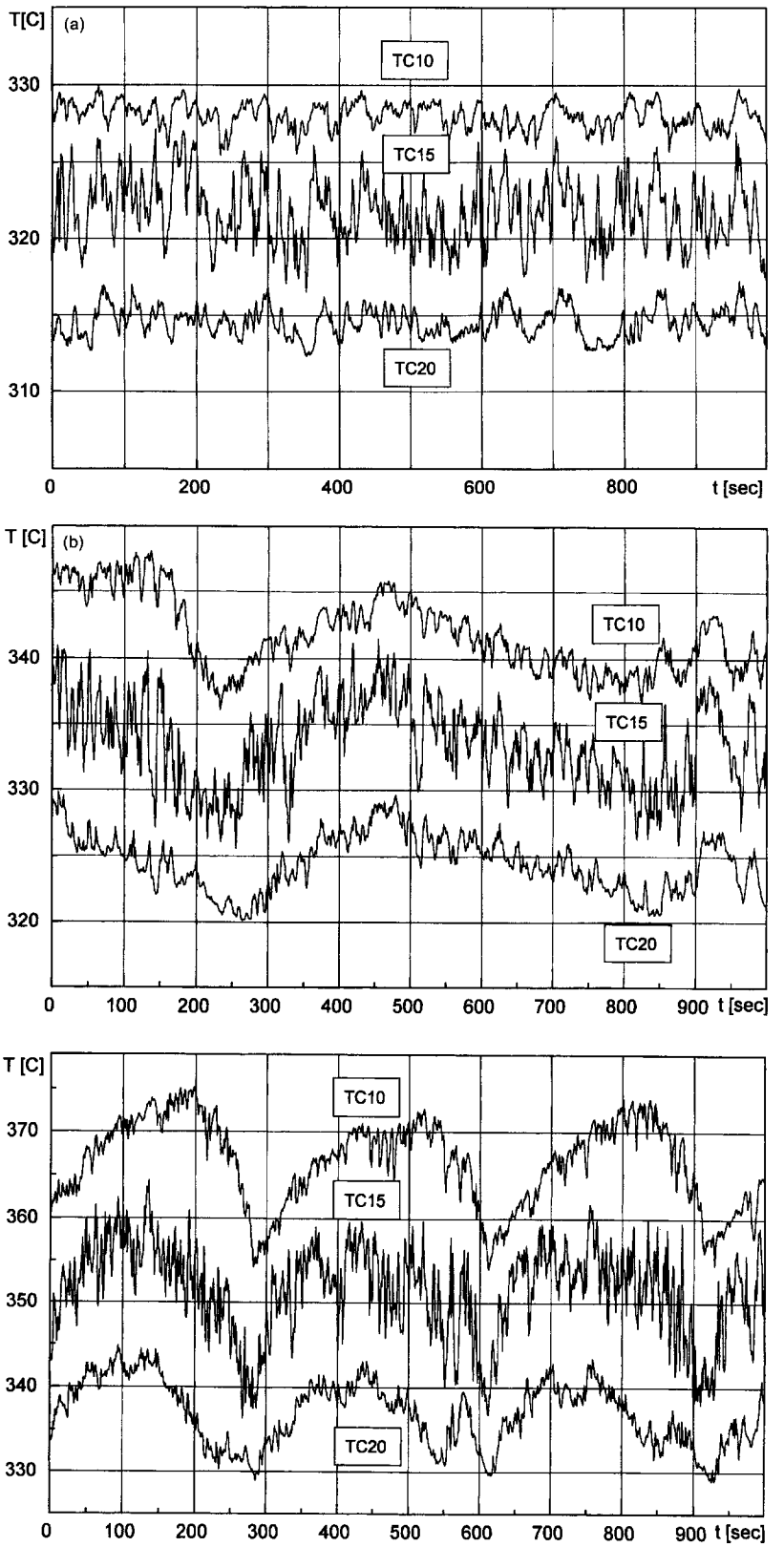

Fig. 10. Temperature histories recorded from thermocouples of TC-rake 2 at the axial positions: surface of heating plate (TC 10), middle of sodium layer (TC 15) and surface of cooling plate (TC 20) for $Ra = 2 \times 10^6$ (a), $Ra = 2.8 \times 10^6$ (b) and $Ra = 4.3 \times 10^6$ (c).

the thermometer at the center of the heating plate (PT11) and the one at the outermost position (PT1) at a distance of 80 mm from the rim. The temperature signals are normalized by the mean temperature averaged over 5000 s and shown in Fig. 11. The two signals are nearly out of phase by 180°. Due to this phase shift of 200–300 s, significant conductive heat fluxes occur within the heating plate. Taking one half of the horizontal extent of the test chamber as the relevant length scale for a conductive equalisation of the temperature and the thermal diffusivity of copper, $\kappa_{cu} = 1.2 \times 10^{-4}$ m^2 s^{-1}, we obtain a time scale of the order $\tau \simeq 100$ s. We conjecture therefore, that the large scale temperature fluctuations are caused by an interaction of the convective heat transport in the sodium and the conductive equalization of temperature fluctuations in the bounding copper plates. The relaxation character of the long term temperature fluctuation recorded by the thermocouple T_{10} and shown in Fig. 10(c) is characteristic for a conduction–convection-controlled process. Relaxation oscillations in Bénard convection were first discussed by Busse [47]. Other possible origins of the long period oscillations such as fluctuations in the thickness of the thermal boundary layer or circulating hot spots can be excluded, since their time scales vary between 1.5 and 6 s.

The intensity of fluctuations, i.e. the temperature RMS value is a characteristic statistical property of a fluctuating temperature field. Fig. 12 shows the RMS values of the temperature distribution across the layer height measured by thermocouples at the rake 2 near the center of the test cell. The plotted values correspond to the mean temperature distributions shown in Fig. 9. The formation of a thermal boundary layer near the lower and upper boundaries of the container can be identified by the emergence of two maxima in the curves fitting the RMS values for Rayleigh numbers $Ra \geq 1.2 \times 10^6$. The unusual high level of the RMS values at the bounding copper plates underlines once more the fact that the thermal boundary conditions are in general not ideal in sodium experiments, even if copper is used as the material for the confining container walls. The normalized RMS values (RMS/ΔT) are plotted in Fig. 13. These values are evaluated from the temperature signals of a thermocouple located at the mid-height of the sodium layer. The graph displays the results from our recent measurements and also RMS values from previous investigations by Kek [18] and Horanyi [39]. After a steep increase the normalized RMS value levels off at between 10 and 20% in the range $3 \times 10^4 < Ra < 4 \times 10^6$. We interpret the lower level of the RMS values in the range $2 \times 10^5 < Ra < 5 \times 10^6$ as an indication of the difference in the flow patterns occurring in two different test sections with layer heights of 25 mm [18,39] and 110 mm (new measurements).

Fig. 14 shows normalized power spectrum density functions (PSD) of the temperature signals E_T which are recorded in the center of the test chamber. The

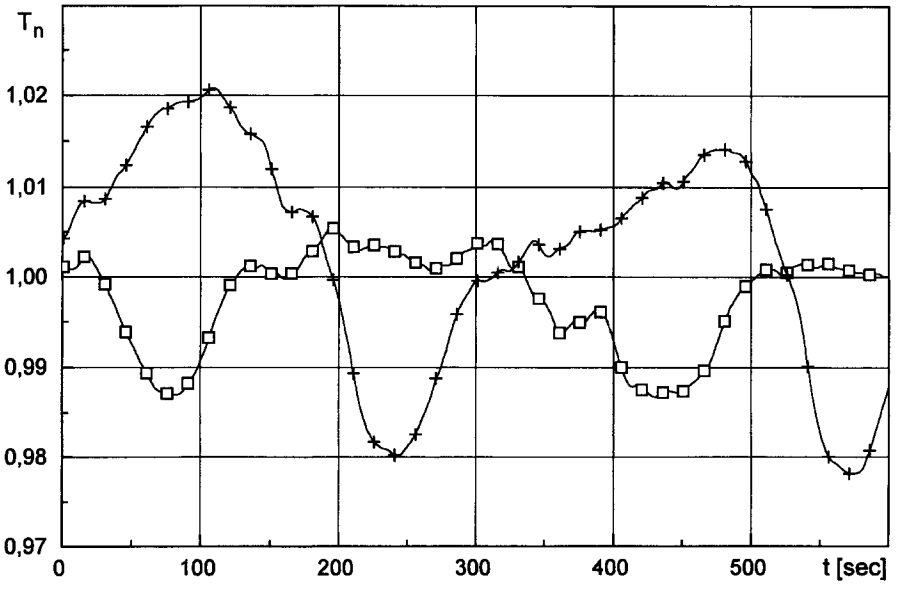

Fig. 11. Normalized temperature histories recorded from Pt-100 thermometers at the positions $r/R = 0$ (□□□), $r/R = 0.7$ (+ + +).

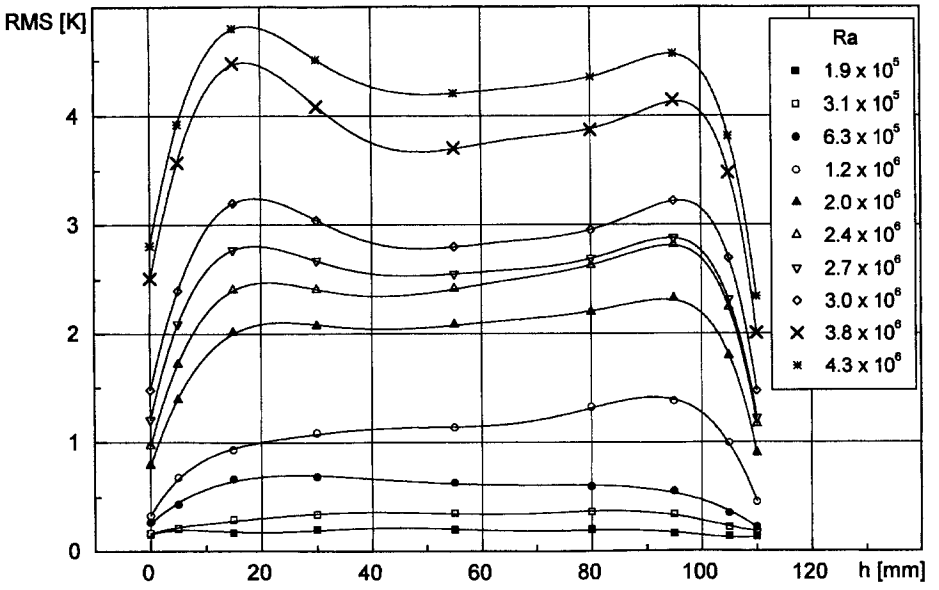

Fig. 12. RMS-profiles of thermocouple signals of TC-rake 2 across the sodium layer for different Rayleigh numbers.

PSD functions are plotted for three different Rayleigh numbers, $Ra = 3.55 \times 10^5$, 1.45×10^6 and 4×10^6. It is seen that the cut-off-frequencies are generally lower than 1.2 Hz but increase with increasing Rayleigh numbers in the range from 8×10^{-2} to 1.2×10^{-1} Hz. All the three spectra decay with nearly the same power of $E_T \sim f^{-4}$. This latter finding is not consistent with the prediction of the spectral model of Batchelor et al. [48] which gives $E_T \sim f^{-17/3}$ for low Prandtl number fluids in the inertial-diffusive subrange of the thermal energy spectrum. This subrange is specified by the Kolmogoroff and Batchelor time scales $\tau_k = (\nu/\epsilon)^{1/2}$

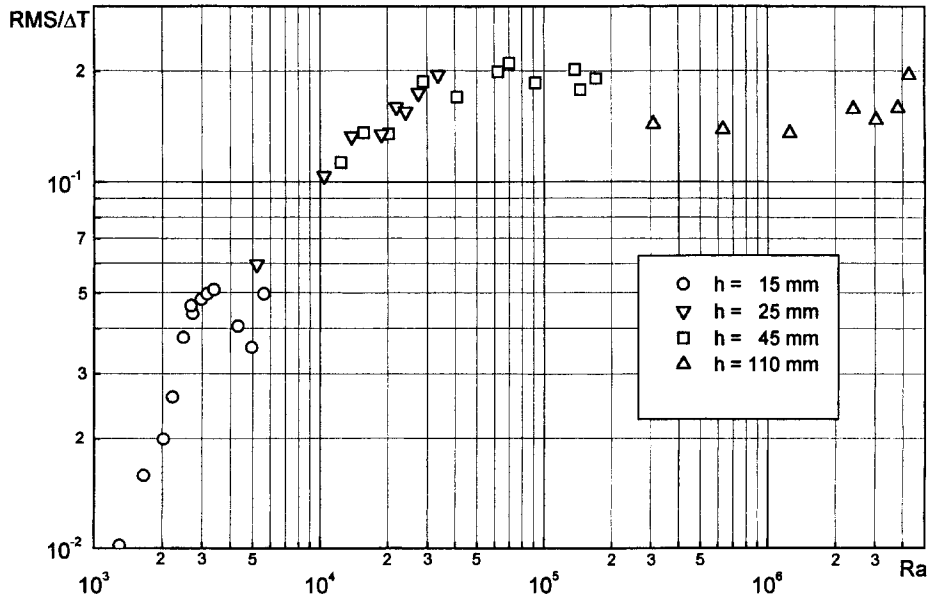

Fig. 13. RMS-values normalized by the mean temperature differences across the sodium layer versus Rayleigh number, evaluated for the aspect ratios 33 (○○○), 20 (▽▽▽), 11 (□□□) and 4.5 (△△△).

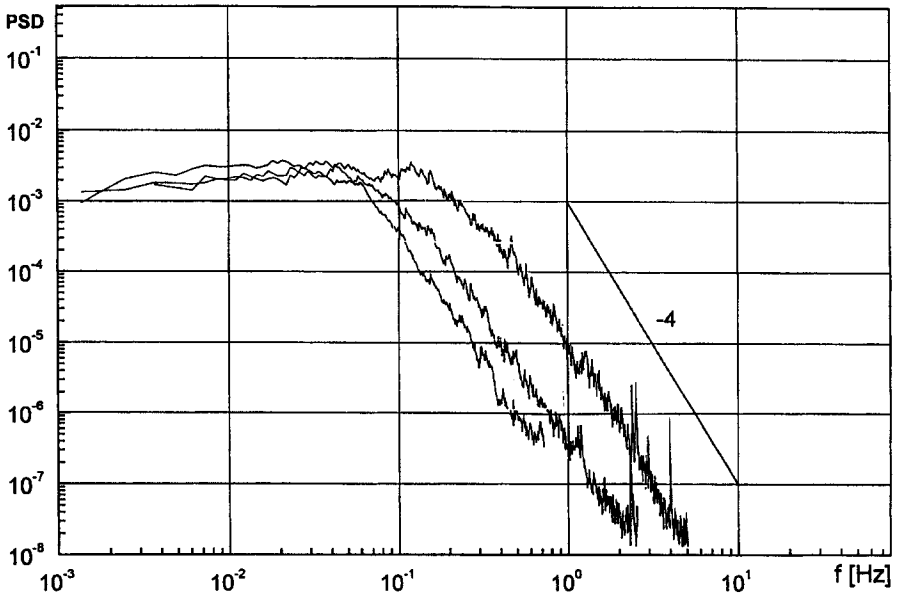

Fig. 14. Normalized power spectrum density functions of TC 15 signals for the Rayleigh numbers $Ra = 4 \times 10^6$ (a), $Ra = 1.5 \times 10^6$ (b) and $Ra = 3.6 \times 10^5$ (c).

and $\tau_B = (\kappa/\epsilon)^{1/2}$, where ν is the kinematic viscosity, κ the thermal diffusivity and ϵ the viscous dissipation.

Using a refined similarity hypothesis by introducing a local length scale based on the strain rate, Gibson [49] derived a spectral relationship $E_T \sim f^{-3}$ in the limit of vanishing Prandtl number, $Pr \to 0$, in a frequency range

$$2\pi \times \nu_b \left(\frac{\epsilon}{\kappa^3}\right)^{1/4} < f < 22\pi \times \nu_b \left(\frac{\epsilon}{\kappa^3}\right)^{1/4} \times Pr^{-1/4}.$$

Here

$$\nu_b = \left(\frac{Ra}{Pr}\right)^{1/2} \frac{\nu}{h}$$

holds in terms of integral parameters.[3]

For $Ra = 4 \times 10^6$ we get $\nu_b = 11.3$ cms^{-1}. Since Gibson's findings for the power decay apply for the limiting case $Pr \to 0$ and a range of considerable higher frequencies, namely for 1.7 s^{-1} < f < 40 s^{-1}, our observed stronger decay relation $E_T \sim f^{-4}$ is unlikely to be related to an interference between the inertial range of the velocity spectrum and the diffusive range of the temperature spectrum. We suggest that the temperature decay occurs predominantly by molecular diffusion in a frequency range where the first generation of energy containing eddies originates from buoyancy release and where vortex generation by energy transfer to smaller size eddies is still negligible. Moreover, for the range of Reynolds numbers 3000 < Re < 30,000, achieved experimentally, the velocity PSD-function may not contain a marked inertial range at all. According to Tennekes and Lumley [50] an inertial subrange exists only for $Re > 10^5$. Here, the Reynolds number is defined as $Re \doteq (Ra/Pr)^{1/2}$.

In his book Hinze ([51], p. 283) outlines for the case of small Prandtl number fluids that the power spectrum density (PSD) of a passive scalar, here the temperature, should scale as $E_T(f, t) = H\kappa^{-3} E(f, t) \times f^{-4}$ in a turbulent velocity field. Here $E(f, t)$ is the PSD function of the velocity field. In the frequency range of the power containing eddies $E(f, t)$ can be assumed constant. Thus, the temperature power spectrum is purely diffusive under these conditions and has an $E_T \sim f^{-4}$ dependency. This seems to be consistent with our observations.[4]

The quality of turbulent flow has frequently been assessed from the character of the probability distribution function (PDF) of fluctuating signals, as for instance of temperature time signals [53]. Figs. 15–17

[3] The discussions of Batchelor et al. [48] and Gibson [49] are originally given in the wave number space. In this paper their results are transformed by Taylor's hypothesis to the frequency space. The equivalence of the normalized wave number and frequency spectra has been demonstrated by Chilla et al. [17]

[4] It is obvious, that the measured spectra do not contain a buoyancy range of influence according to Bolgiano [52] with a behavior of $\epsilon_T \sim k^{-7/5}$ as discussed by Cioni et al. [11].

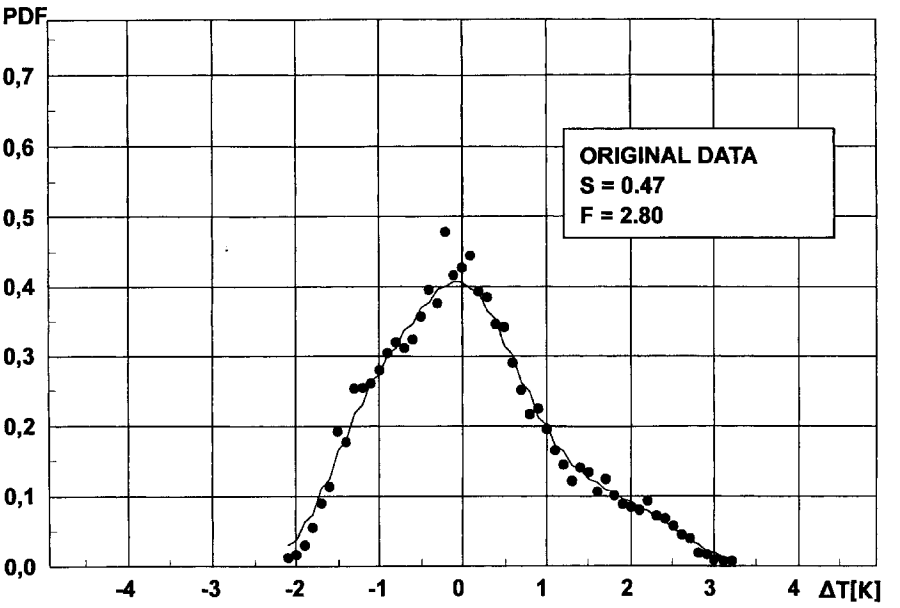

Fig. 15. Normalized probability density function of temperature signal of TC15 (original data) for $Ra = 3.6 \times 10^5$.

show normalized PDFs for Rayleigh numbers $Ra = 3.5 \times 10^5$, 1.45×10^6, 4×10^6. The PDFs were evaluated from temperature signals recorded by the thermocouple TC15 of rake probe 2 in the middle of the sodium layer and thermocouple TC10 on the surface of the heating plate.

The PDFs for Rayleigh numbers $Ra = 3.5 \times 10^5$, $Ra = 1.45 \times 10^6$ (signals are recorded from the thermocouple TC15 in the middle of the sodium layer) are shown in Figs. 15 and 16. They exhibit a significant asymmetry with skewness of opposite sign ($S = 0.47$ and $S = -0.46$, respectively). The change of sign in the skewness is another indication of the change of the overall mode of convection from down flow to upflow in the center of the test chamber. In general, there is an obvious trend in the small scale fluctuations from

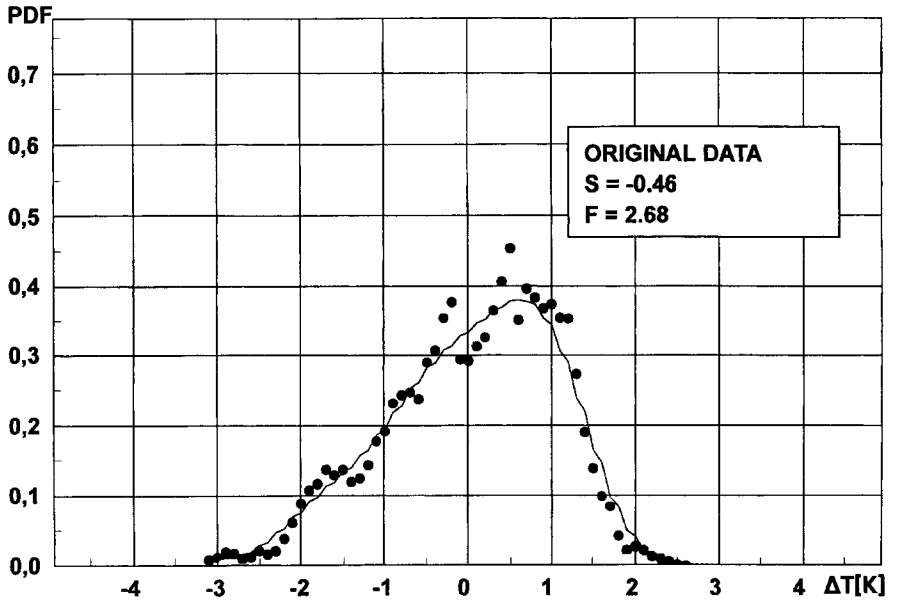

Fig. 16. Normalized probability density function of temperature signal of TC15 (original data) for $Ra = 1.5 \times 10^6$.

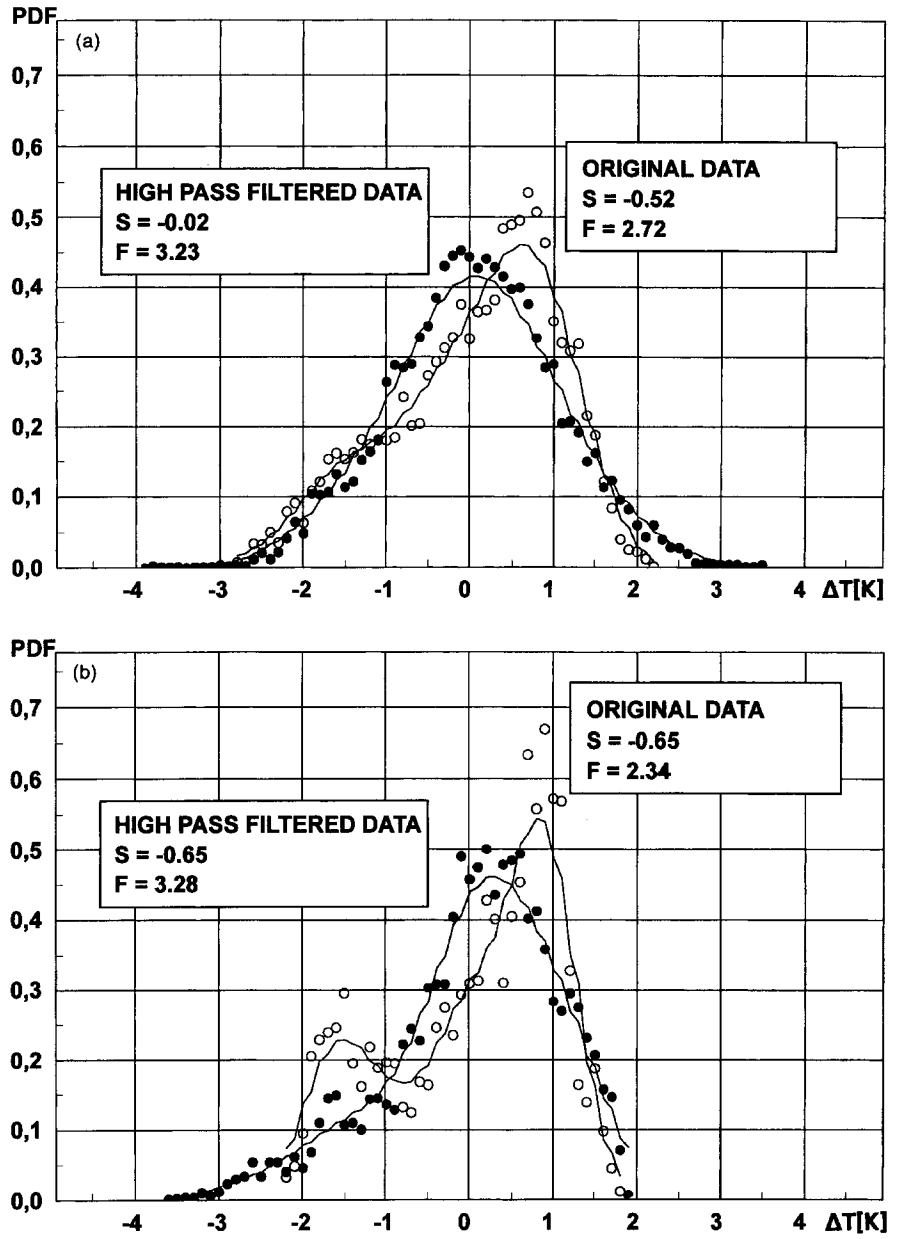

Fig. 17. Normalized probability density functions of temperature signals of TC15 (a) and TC10 (b) for $Ra = 4 \times 10^6$. Comparison of original (○) and high pass filtered (●) data.

an asymmetric distribution towards a symmetric quasi Gaussian distribution in the bulk flow with increasing power level, i.e. increasing Rayleigh numbers.

For a high Rayleigh number $Ra = 4 \times 10^6$ the PDF of the unfiltered temperature signal TC15 results also in a skewed distribution. This can be seen in Fig. 17(a). When the low frequency content of the temperature signal is filtered by a high pass filter with a cut-off-frequency of 2×10^{-2} Hz the PDF becomes a nearly Gaussian distribution with a very low skewness, $S = 0.02$, and a flatness of $F = 3.2$. This indicates that a uniform small scale fluctuation 'rides' on a very long period, large scale motion. The Gauss like distribution of the filtered signal suggests, that a quite regularly structured, weakly turbulent convection exists for Rayleigh numbers of the order 10^6 which Castaing et al. [4] term 'soft turbulence'. It is obvious from the filtering process, that the skewness $S = -0.52$ of the unfiltered signal originates from the oscillatory, low frequency content of the temperature signal. For the

same reason the flatness value drops below $F < 3$. Compared with the higher frequency parts of the signal the large scale fluctuating motion becomes even more evident, when the temperature time signal is evaluated for thermocouples at the heating or cooling plate. The PDF function is presented in Fig. 17(b) for a temperature signal at the cooling plate (see Fog. 10(c), TC10). The unfiltered signal shows two clear peaks, the smaller one reflecting the quasi periodic long term oscillation of the overall signal. Both, the filtered and the unfiltered signal have a skewness of $S = -0.65$ but they differ by the flatness which becomes $F = 3.3$ for the filtered signal and $F = 2.3$ for the unfiltered signal. $F = 3.3$ still reflects the Gaussian similarity of the small scale fluctuations but because of the proximity of the hot wall some intensive cold spikes within a rising mean flow result in a significant skewness of $S = -0.65$.

More skewed distributions are observed near the outer edge of the thermal boundary layer. This can be seen in Fig. 18(a), which shows the distribution of skewness across the layer height at the position of the thermocouple rake 2. The corresponding flatness distribution for the same conditions are given in Fig. 18(b). The values at Rayleigh number $Ra > 10^6$ seem to center around $F \approx 2.5$; this value is noticeably smaller than $F = 3$ for the Gaussian distribution. This indicates that the temperature signal in the center of the test chamber has become voided of short pulsed temperature spikes whereas the slow oscillatory content of the temperature signals remain undamped. This is reasonable as temperature disturbances generated in the boundary layers lose their identity by thermal dissipation along their path of transportation.

5. Discussion and conclusions

Our recent sodium experiment in a cylindrical test chamber of aspect ratio 4.5 is characterised by an axisymmetric large scale convection in form of two concentric ring cells (see Fig. 7). For low Rayleigh numbers $Ra < 10^5$ down flow has been observed in the center of the test chamber. A pronounced transition to a velocity field with up flow in the center occurs in a Rayleigh number range $1 \times 10^6 < Ra < 2 \times 10^6$. A thermal boundary layer forms at the heating and cooling plate simultaneously with this transition. An evaluation of the local Rayleigh numbers in the thermal boundary layer indicates that this layer becomes unstable at an overall Rayleigh number $Ra > 2.4 \times 10^6$, first at the heating plate and at higher values Ra also

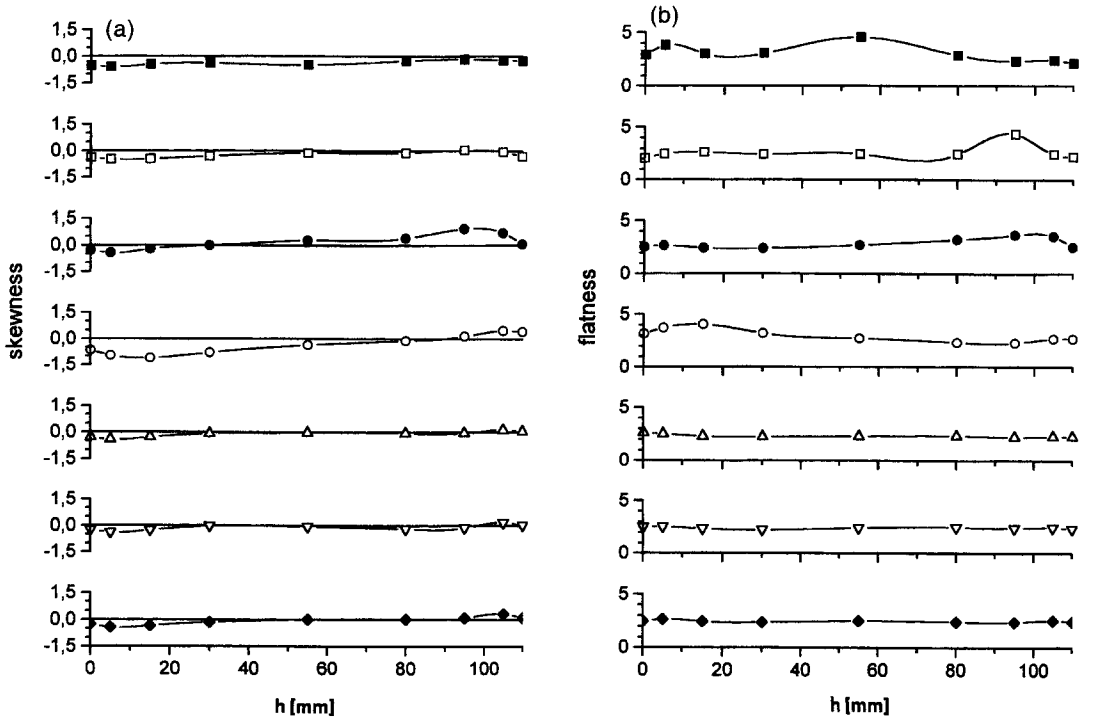

Fig. 18. Profiles of skewness (a) and flatness (b) for different Ra across the sodium layer at the position of TC-rake 2. The different symbols in the graph: ■, □, ●, △, ▽, ◆, refer to the Rayleigh numbers: $Ra = 1.9 \times 10^5$, 3.1×10^5, 6.3×10^5, 1.2×10^6, 2.4×10^6, 2.7×10^6, 3.0×10^6.

at the cooling plate. These thermal instabilities seem to trigger a large scale, long term relaxation oscillation of the overall convective flow. We interpret this phenomenon as a conduction controlled process governed by the comparable heat conductivities of the test fluid sodium and the confining copper boundaries.

The observed temperature fluctuations in a Rayleigh number range $Ra < 10^6$, where pronounced temperature boundary layers do not exist are mainly controlled by instabilities of the velocity field and the thermal diffusion of slight local temperature inhomogenities. The temperature behaves as a passive scalar. This passive behavior of the temperature field is confirmed by the strong spectral decay of the temperature fluctuations with a power law $E_T \sim f^{-4}$ as demonstrated in Fig. 14. The passive character of the temperature field is continued even into the thermally unstable range of the temperature boundary layers up to Rayleigh numbers $Ra \sim 4 \times 10^6$. As the turn around time for the large scale velocity field at high Rayleigh numbers $Ra > 10^6$ is smaller or, at most, of the same order as the formation of thermal instabilities of the temperature boundary layer, the temperature inhomogenities are quickly carried along with the fluid flow, wherein they lose their identity by thermal dissipation. There is no indication of an interaction between the velocity and the temperature fluctuation field; nor is there any signature of a direct influence of the gravity field on thermal inhomogenities. This is clearly recognized from the absence of inertia or buoyancy influenced subranges with $E_T \sim f^{-5/3}$ and $E_T \sim f^{-7/5}$, respectively, in the power density spectra of the temperature in Fig. 14. This is not surprising as the actual velocities in the test chamber result only in Reynolds numbers $Re < 30{,}000$. These values are too low to generate inertial effects in the spectral decay of the kinetic energy of eddies generated by hydrodynamic instabilities [50]. The energy in the velocity field is therefore mainly tied to the large scale, buoyancy induced roll vortices and to relatively well ordered low mode fluid dynamic instabilities of shear flows in the wall regions or to the local oscillations of unstable detaching flows near the free vertical boundaries of the convection cells. One also has to keep in mind the wave-like instabilities along the convection rolls in low Prandtl-number flows described by Busse [54]. These relatively soft fluctuations of the velocity field are reflected in the nearly Gaussian character of the probability density functions observed in our experiments for the temperature signals recorded in the whole range of Rayleigh numbers achieved. Castaing et al. [4] introduced the notation 'soft turbulence' for this type of fluctuating flow governed by a relatively small number of instability modes, which in the case of a closed flow are likely to be characterized by a finite number of discrete wave-lengths giving rise to chaotic interactions.

If one accepts—as suggested above—the existence of two slowly fluctuating concentric ring cells in the test chamber filled with a very low Prandtl number fluid there will be pronounced 'fly wheel' effects in the velocity field. The quasi rigid body rotation in such well-ordered convection cells has frequently been demonstrated by numerical simulations [24,55,56]. Although the so far known numerical calculations are two-dimensional approaches and limited to smaller Rayleigh numbers ($Ra < 20{,}000$), the general features of such 'fly wheel' velocity patterns are reflected in the Nusselt–Rayleigh number correlation for the heat transfer, which according to Busse and Clever [24] should correlate for $(Ra\ Pr)^{1/2} \gg 1$ as $Nu \sim Ra^{1/4}$. Our measurements follow this relationship in a wide range of Rayleigh numbers $2 \times 10^4 < Ra < 5 \times 10^6$. Our experimental set up and consequently the observed large scale flow pattern differs from findings of other authors like Castaing et al. [4], Sano et al. [34], Cioni et al. [8], Takeshita et al. [13] as these experimenters work with cylindrical test chambers of aspect ratio $d/h = 1$. These authors maintain the same single convection roll, which is oriented with its axis along the container diameter and which may rotate in azimuthal direction for the whole range of Rayleigh numbers. In general one may speculate, that the fluid dynamic instability modes they encounter are less numerous compared with the instabilities of our concentric ring roll system. Nevertheless, in the low Rayleigh number range and with mercury as a test fluid the overall features of the perturbations are similar, namely determined by two kinds of instabilities, the hydrodynamic fluctuating instabilities of low Prandtl number flows in a thermally stratified environment [54] and the thermal instabilities of temperature boundary layers. There is a noticeable difference between the experiments in mercury and in sodium with $Pr = 0.025$ and $Pr \simeq 0.006$, respectively. The measured heat transfer correlation in terms of a power law $Nu \sim Ra^m$ in mercury show a persistently higher value of m, namely $m = 0.26$ [21,12] and $m = 0.286$ [13] compared with our value of $m = 0.25$. However, the measurements were taken in different Rayleigh number ranges, for mercury in the range $10^6 < Ra < 10^9$ and for sodium in $10^4 < Ra < 5 \times 10^6$. As the power relations reflect the different physical mechanisms of heat transport, the 'mixing layer' model of Castaing et al. [4] on the one hand and the 'fly wheel' model of Jones et al. [2] on the other hand, further experimental work is desirable to decide on the validity of the two different physical ideas.

In summary, the present available experimental data of different authors for the convective heat transfer for different fluids ranging from silicon oil to sodium and Prandtl numbers varying between $Pr \sim 10^3$ and $\sim 10^{-3}$ are compiled in the O'Toole and Silveston [57] graph

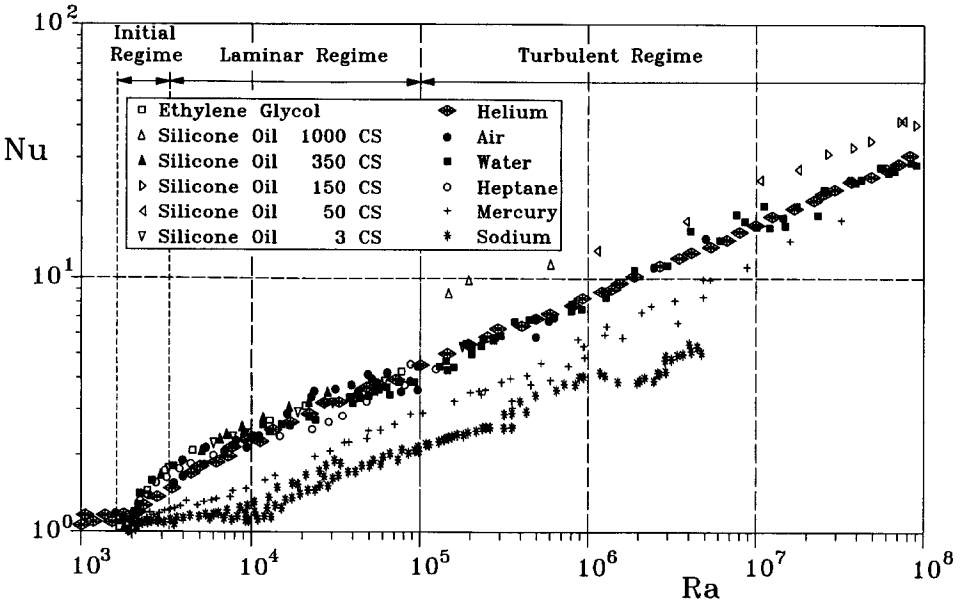

Fig. 19. Heat transfer data $Nu(Ra)$ summarized in an O'Toole and Silveston graph.

of Fig. 19. It is quite obvious, the Nusselt number decreases at all Rayleigh numbers monotonically with the Prandtl number. There is as yet no general relationship available based on physical reasoning to describe and explain the overall correlation between the essential dimensionless groups of convective heat transfer, namely *Nu, Ra* and *Pr*.

Acknowledgements

The authors gratefully acknowledge critical and constructive comments on a draft of this article by S. Cioni and J. Sommeria which contributed significantly to its improvement. They also gratefully appreciate practical advice from R. Kayulla during the performance of the experiments.

References

[1] E. Siggia, High Rayleigh number convection, Ann. Rev. Fluid Mech. (1994).
[2] C.A. Jones, D.N. Moore, N.O. Weiss, Axisymmetric convection in a cylinder, J. Fluid Mech. 73 (1976) 353–388.
[3] R. Vercicco, R. Camussi, Transitional regimes of low-Prandtl thermal convection in a cylindrical cell, Phys. Fluids 9 (5) (1997) 1287–1295.
[4] B. Castaing, G. Gunaratne, F. Heslot, L. Kadanoff, A. Libchaber, S. Thomae, X.Z. Wu, St Zaleski, A. Zanetti, Scaling of hard thermal turbulence in Rayleigh–Bénard convection, J. Fluid Mech. 204 (1989) 1–30.
[5] F. Heslot, B. Castaing, A. Libchaber, Transition to turbulence in helium gas, Phys. Rev. A 36 (1987) 5870–5873.
[6] A. Tilgner, A. Belmonte, A. Libchaber, Temperature and velocity profiles of turbulent convection in water, Phys. Rev. E 47 (1993) 2253–2256.
[7] T.H. Salomon, J.P. Gollub, Sheared boundary layers in turbulent Rayleigh–Bénard convection, Phys. Rev. Lett. 64 (1990) 2382–2385.
[8] S. Cioni, S. Horanyi, L. Krebs, U. Müller, Temperature fluctuation properties in sodium convection, Phys. Rev. E 56 (4) (1997) 3753–3756.
[9] R. Krishnamurti, Low frequency oscillations in turbulent Rayleigh–Bénard convection: laboratory experiments, Fluid Dyn. Res. 16 (1995) 87–108.
[10] R.J. Goldstein, H.D. Chiang, D.L. See, High-Rayleigh number convection in a horizontal enclosure, J. Fluid Mech. 213 (1990) 111–126.
[11] S. Cioni, S. Cilimberto, J. Sommeria, Temperature structure functions in turbulent convection at low Prandtl number, Europhys. Lett. 32 (5) (1995) 413–418.
[12] S. Cioni, S. Ciliberto, J. Sommeria, Strongly turbulent Rayleigh–Bénard convection in mercury: comparison with results at moderate Prandtl number, J. Fluid Mech. 335 (1997) 111–140.
[13] T. Takeshita, T. Segawa, J.A. Glazier, Mo Sano, Thermal turbulence in mercury, Phys. Rev. Lett. 76 (1996) 1465–1468.
[14] V. Yakot, Correspondence principle for turbulence: application to the Chicago experiments on high Rayleigh number Bénard convection, Phys. Fluids A 1 (1989) 175–178.
[15] J.B. Shraiman, E.D. Siggia, High transport in high-Rayleigh-number convection, Phys. Rev. A 42 (1990) 3650–3653.
[16] X.-Z. Wu, L. Kadanoff, A. Libchaber, S. Masaki,

Frequency power spectrum of temperature fluctuations in free convection, Phys. Rev. Lett. 64 (1990) 2140–2143.
[17] H. Chilla, S. Ciliberto, C. Innocenti, E. Pampaloni, Boundary layer and scaling properties in turbulent thermal convection, Il Nuovo Cimento 15D (1993) 1229–1249.
[18] V. Kek, Bénard–Konvektion in flüssigen Natriumschichten, Dissertation, Universität Karlsruhe, 1989.
[19] V. Kek, U. Müller, Low Prandtl number convection in layers heated from below, Int. J. Heat Mass Transfer 36 (1993) 2795–2804.
[20] S. Globe, D. Dropkin, Natural-convection heat transfer in liquids confined by two horizontal plates and heated from below, J. Heat Transfer (1959).
[21] T.H. Rossby, A study of Bénard convection with and without rotation, J. Fluid Mech 36 (1969) 309–335.
[22] J. McDonald, T.J. Connolly, Investigations of natural convection heat transfer in sodium, J. Nucl. Sci. Engng 8 (1960) 369–377.
[23] R.H. Kraichnan, Turbulent thermal convection at arbitrary Prandtl number, Phys. Fluids 5 (1962) 1374–1389.
[24] F.H. Busse, R.M. Clever, An asymptotic model of two-dimensional convection in the limit of low Prandtl number, J. Fluid Mech. 102 (1981) 75–83.
[25] D.C. Threllfall, Free convection in low-temperature gaseous helium, J. Fluid Mech. 67 (1975) 17–20.
[26] X. Chavanne, F. Chilla, B. Castaing, B. Hébral, B. Chabaud, J. Chaussy, Observation of the ultimate regime in Rayleigh–Bénard convection, Phys. Rev. Lett. 79 (1997) 3598–3651.
[27] J.W. Deardorf, G.E. Willis, Investigation of turbulent thermal convection between horizontal plates, J. Fluid Mech. 28 (1967) 675–704.
[28] R.J. Goldstein, T.Y. Chu, Thermal convection in a horizontal layer of air, Prog. Heat and Mass Transfer 2 (1969) 55–75.
[29] T.Y. Chu, R.J. Goldstein, Turbulent convection in a horizontal layer of water, J. Fluid Mech. 60 (1973) 141–159.
[30] E.F.C. Somerscales, J.W. Gazda, Thermal convection in high Prandtl number liquids at high Rayleigh numbers, Int. J. Heat Mass Transfer 12 (1969) 1491–1511.
[31] A.M. Garon, R.J. Goldstein, Velocity and heat transfer measurements in thermal convection, Phys. Fluids 16 (1973) 1818–1825.
[32] Y. Kikuchi, T. Shioyama, Z. Zawara, Turbulent heat transport in a horizontal fluid layer heated internally and from below, Int. J. Heat Mass Transfer 29 (1986) 451–461.
[33] H. Tanaka, H. Miyata, Turbulent natural convection in a horizontal water layer heated from below, Int. J. Heat Mass Transfer 23 (1980) 1273–1281.
[34] M. Sano, X.Z. Wu, A. Libchaber, Turbulence in helium-gas free convection, Phys. Rev. A 40 (1989) 6421–6430.
[35] G.E. Willis, J.W. Deardorf, Development of short-period temperature fluctuations in thermal convection, Phys. Fluids 10 (1967) 931–937.
[36] K. Bremhorst, L. Krebs, U. Müller, J.B.H. Listijono, Application of a gradient diffusion and dissipation time scale model for prediction of mean and fluctuating temperature fields in liquid sodium downstream of a multi-bore jet block, Int. J. Heat Mass Transfer 11 (1989) 2037–2046.
[37] J.L. Lumley, Stochastic Tools in Turbulence, Academic Press, 1970.
[38] PlotIT, Commercial computer software published: Scientific Programming Enterprises, 1990.
[39] S. Horanyi. Unpublished Report-FZK, 1994.
[40] E.L. Koschmieder, S.G. Pallas, Heat transfer through a shallow horizontal convecting fluid layer, Int. J. Heat Mass Transfer 17 (1974) 991–1002.
[41] K. Stork, U. Müller, Convection in boxes: an experimental investigation in vertical cylinders and annuli, J. Fluid Mech. 71 (1975) 231–240.
[42] V. Steinberg, G. Ahlers, S. Cannell, Pattern formation and wave-number selection by Rayleigh–Bénard convection in a cylindrical container, Physica Scripta 32 (1985) 534–547.
[43] A.X. Zhao, F.C. Moates, R. Narayanan, Rayleigh convection in a closed cylinder—experiments and a three dimensional model with temperature-dependent viscosity effects, Phys. Fluids 7 (7) (1995) 1576–1582.
[44] C. Mika, Messungen der Strömungsgeschwindigkeit in beheizten Kühlkanälen aus der Korrelation flukturierender Temperatursignale, Dissertation, Technische Universität Hannover, 1975.
[45] C. Koppermann, Geschwindigkeits- und Durchflußmessung in einphasigen Strömungen mit Kreuzkorrelationsverfahren, Dissertation Universität Karlsruhe, Fortschr.-Ber. VDI-Z 8, 63, 1983.
[46] J.N. Koster, U. Müller, Oscillatory convection in vertical slots, J. Fluid Mech. 139 (1984) 363–390.
[47] F.H. Busse, Non-stationary finite amplitude convection, J. Fluid Mech. 28 (1967) 223–239.
[48] G.K. Batchelor, I.D. Howless, A.A. Townsend, Small-scale variation of convected quantities like temperature in turbulent fluid. The case of large conductivity, J. Fluid Mech. 5 (1959) 134–139.
[49] C.H. Gibson, Fine structure of scalar fields mixed by turbulence II spectral theory, Phys. Fluids 11 (1968) 2316–2327.
[50] H. Tennekes, J.L. Lumley, A First Course in Turbulence, MIT Press, Cambridge, 1974.
[51] J.O. Hinze, Turbulence, McGraw-Hill, 1975.
[52] R. Bolgiano, Turbulent spectra in a stably stratified atmosphere, J. Geograph. Res. 64 (1959) 2226–2228.
[53] F. Heslot, A. Belmonte, A. Libchaber, Temperature and velocity profiles of turbulent convection in water, Phys. Rev. E 47 (1993) R2253–R2256.
[54] F.H. Busse, The oscillatory instability of convection rolls in low Prandtl number fluid, J. Fluid Mech. 52 (1972) 97–112.
[55] R.M. Clever, F.H. Busse, Nonlinear oscillatory convection, J. Fluid Mech. 176 (1987) 403–417.
[56] B. Mundinger, Numerische Simulation einer Konvektionsströmung in einer Zylinder-geometrie, Diplomarbeit Universität Karlsruhe, 1989.
[57] J.L. O'Toole, P.L. Silveston, Correlations of convective heat transfer in confined horizontal layers, Chem. Engng Prog. Symp. Ser. 67 (1961) 81–86.